Lateral Templating for Guided Self-Organization of Sputter Morphologies**

By *Alexandre Cuenat*, *H. Bola George*, *Kee-Chul Chang*, *Jack M. Blakely*, and *Michael J. Aziz**

Methods for the fabrication of large areas of nanoscale features with controlled period and intraperiod organization are of interest because of the potential for high-throughput mass production of nanoscale devices. Due to their potential in this regard, much recent attention has been devoted to self-organization processes,[1–5] in which processing causes the spontaneous emergence of a nanoscale pattern. The short-range order can be quite high[2–4] but some envisaged applications require long-range order, which is destroyed by uncontrolled topological defects arising spontaneously from the self-organization process. A potentially successful hierarchical fabrication strategy is the fabrication of controlled features at a small, but lithographically tractable, length scale by methods such as conventional mask or optical-standing-wave lithography, in order to guide a self-organization process at the finest length scale.[6–8] Topographic patterning has been used for templating the local disorder in two-dimensional (2D) self-assembled monolayers[9] and for templating defect organization or elimination in three-dimensional (3D) colloidal crystallization.[10] Topography has also been used to manipulate semiconductor quantum-dot placement, composition, and strain, through its effect on stress,[11] surface energy, and mobility.[12] 3D short-range ordering of grown-in quantum-dot short-period superlattices can result from multilayer growth;[1,4] nanoscale topographic templating of the first layer could dramatically accelerate the development of order and lead to true long-range order. Lithographically and focused ion beam (FIB)-patterned topographies have recently been used to template quantum-dot growth in linear chains,[8] periodic 2D lattices,[7] and in more complex configurations that are promising for novel nanoelectronic architectures, such as quantum cellular automata.[13] The finest features have been templated by serial writing with a FIB, a prohibitively expensive process for mass production that might be circumvented by using a hierarchical fabrication strategy. Here we report the influence of patterned boundaries on the primary material of complementary metal oxide semiconductor (CMOS) technology, i.e., a Si(001) substrate, in guiding self-organized topographic ripples spontaneously appearing during uniform irradiation with low energy Ar^+ ions. We show that the long-range order of the features can be greatly enhanced by this lateral-templating approach. The emerging pattern can be manipulated by changing the boundary spacing and misorientation with respect to the projected ion-beam direction. We develop a scalar figure of merit, a dimensionless topological defect density, to characterize the degree of order of the pattern. At small boundary separation, greatest order is observed when the separation is near an integer multiple of the spontaneously arising feature size. The defect density is exceedingly low up to a critical misorientation angle, beyond which topological defects develop in proportion to the incremental misorientation. These results suggest the potential utility of lateral templating ion-irradiation-induced topographic patterns for high-throughput fabrication at sublithographic length scales.

Sputter patterning is the spontaneous formation of one- and two-dimensional arrays of topographical ripples and dots on the surfaces of solids eroded by a directed ion beam. This phenomenon has been observed for a wide range of ion species, energies, and incident angles on a variety of materials, including glass,[14] semiconductors,[3,15–17] metals,[18] and insulators.[19] Spontaneously emerging feature sizes, which are selected by the kinetics and, consequently, are continuously tunable via the operating conditions, have been reported[3] as small as 15 nm. In general, controlling the behavior of such driven systems is important in many areas of science and engineering.[20] The success of lateral templating raises the possibility of controlling the morphology at a fine length scale in mass production. Because ion irradiation is currently used for doping control in the mass production of semiconductor devices, there may be little impediment to its rapid uptake for morphology control. We investigate the control of the self-organized sputter pattern by using lithography to control only the boundaries of the field over which morphological features evolve.

The system chosen for study was silicon with argon-ion irradiation under conditions known to create a topographically rippled surface with small ordered domains at a spontaneously arising "natural" wavelength of $\lambda = 140$ nm. Details are reported in the Experimental section. The morphological development of templated and non-templated regions was compared after exposure under identical conditions. Figure 1a shows an atomic force microscopy (AFM) topograph of a templated substrate after ion bombardment. The initial configuration consists of a series of 200 nm mesas and 200 nm valleys with a periodicity of 400 nm, as shown in the top trace in Figure 1b. Figure 1a and the bottom trace of Figure 1b

[*] Prof. M. J. Aziz, H. B. George, Dr. A. Cuenat[+]
Division of Engineering and Applied Sciences, Harvard University
Cambridge, MA 02138 (USA)
E-mail: maziz@harvard.edu
Dr. K.-C. Chang,[++] Prof. J. M. Blakely
Materials Science Center, Cornell University
Ithaca, NY 14853 (USA)

[+] Present address: Nano and Functional Materials, Division of Engineering, National Physical Laboratory, Middlesex, England, UK.

[++] Present address: Materials Science Division, Argonne National Laboratory, Argonne, IL 60439, USA.

[**] The authors gratefully acknowledge Dimitris Papazoglou for helpful discussions on image analysis. This research was supported by the U.S. Department of Energy under DE-FG02-01ER45947 and by the Harvard MRSEC under NSF-DMR-0213805. K. C. and J. B. were supported by NSF grant DMR-0109641 and by the Cornell MRSEC. A. C. and H. B. G. contributed equally to the work reported here.

 DOI: 10.1002/adma.200500717

ADVANCED MATERIALS

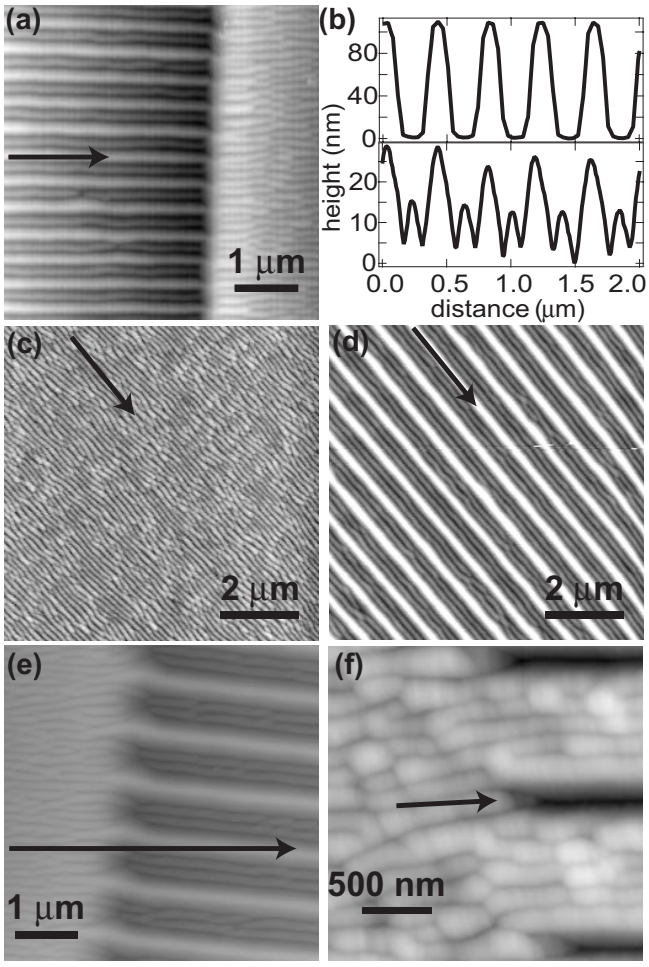

Figure 1. Si(001) sputter-ripple morphologies. Arrows indicate direction of projected ion beam. a) Lithographically templated substrate after bombardment with 1 keV Ar^+ at 540 °C. A single sputter ripple has formed in each valley between the template walls. The boundary of the pre-patterned region separates regions where few (left-hand side of image) and many (right-hand side of image) topological defects are formed. Wavelength of spontaneously arising ripples, $\lambda = 140$ nm, template valley bottom = 200 nm. b) AFM line scans across templated ridges before irradiation (top) and after irradiation (bottom). c) Self-organized ripples formed far from the template, and d) in the presence of a lithographically defined template with 430 nm valley bottom. e) Deflection of ripple orientation by the template. Ripples in valleys follow the boundary rather than the ion beam. f) Organization of Ar^+ sputter ripples on mesas between FIB-milled trenches.

show the resulting topography after irradiation. The right-hand side of the image in Figure 1a shows ripples on the non-templated part of the sample. The ripples meander along the projected ion-beam direction with frequent bifurcation in "dislocation-like" defects. This is the typical structure of self-organized ripples on a "normal", initially flat Si(001) surface. The pre-patterned portion, the left-hand side of Figure 1a, exhibits straight ripples with almost no defects in the bottom of the lithographically defined valleys. In this case only one ripple is formed between patterned boundaries due to the narrow valley width. The height of the ripples in the bottom of the valley is about 10 nm, whereas the height of the remaining initial pattern shrinks from 110 to about 30 nm. This observation suggests that, under appropriate sputtering conditions, one might obtain a spontaneously arising feature height equal to the height of the written boundaries.

Figures 1c,d show the result of increasing the spatial period of the patterned template until two ripples fit in each valley between the mesas. Figure 1c shows self-organized ripples on an initially featureless substrate, just outside the patterned region. The pattern is replete with topological dislocations. Figure 1d shows a templated part of the same sample, with the template pattern originally consisting of mesas 240 nm wide and valleys 430 nm wide. The regularity of these "guided" self-organized ripples is dramatically improved by the template. In Figure 1e we show the result of small deviations of the template direction from the direction of the projected ion beam. The ripples follow the boundary rather than the projected ion beam or the surface crystallography. In Figure 1f we demonstrate the organization of ripples along mesa tops when trenches are milled with a Ga^+ FIB. Ar^+ irradiation was carried out for 65 min in this case. We observed five ripples per mesa with some defects, but the order is nevertheless greatly improved over the ordering of the ripples in the adjacent non-templated area.

Ordering is very much enhanced by confining the sputter-patterned area within the boundaries of a template. To quantify the degree of order we developed an algorithm for determining the normalized density (N_D) of topological defects, as a scalar figure of merit. For a given image, N_D was found to be invariant to pixel resolution if the ratio of the pixel size to the natural ripple wavelength λ was greater than 0.15. Consequently, each image analyzed was transformed so that the pixel size fell between 0.19 and 0.24λ. For a given image, the pixel resolution was changed by reducing the number of pixels using WSxM scanning probe microscopy software.[21] The resulting text files were opened in ImageJ (image processing and analysis program),[22] reduced from 32- to 8-bit images, and saved as tagged image file format (TIFF) files. Gray-level topographic images $h(x,y)$ were flattened by subtracting a quadratic background in x and y, and reduced to binary black–white images using a threshold, θ, determined by Otsu's method,[23] which uses an iterative algorithm to select the threshold gray level that minimizes the within-group (weighted-summed) variance, σ^2_W, of pixel intensities below and above the threshold,

$$\sigma^2_W(\theta) = n_0(\theta)\sigma^2_0(\theta) + n_1(\theta)\sigma^2_1(\theta) \quad (1)$$

where n_i denotes the probabilities of gray levels within each group and σ^2_i is the variance. The subscripts 0 and 1 represent the levels below and above the threshold, respectively. Thus, if $h(x,y)$ takes values between 0 (black) and 255 (white), the corresponding threshold version is given by $g(x,y) = 255$ if $h(x,y) > \theta$; $g(x,y) = 0$ otherwise. For patterned samples, the template walls were "cut out" manually, i.e., $g(x,y)$ was set to 0, prior to determining the threshold value; otherwise, the results were dominated by the topography of the templates, as

was also the case when attempts were made to characterize ripple order in Fourier space. Binary images were reduced to line traces using the Matlab "thin" function—an operation that shrinks white regions to lines a single pixel in width. The thinned counterparts of the AFM topograph (Fig. 1d) are shown in Figures 2a,b, respectively. In the thinned image, topological defects appear as junctions or line segment ends. From the thinned image, the raw number of these defects was obtained by recording the number of white pixels with other

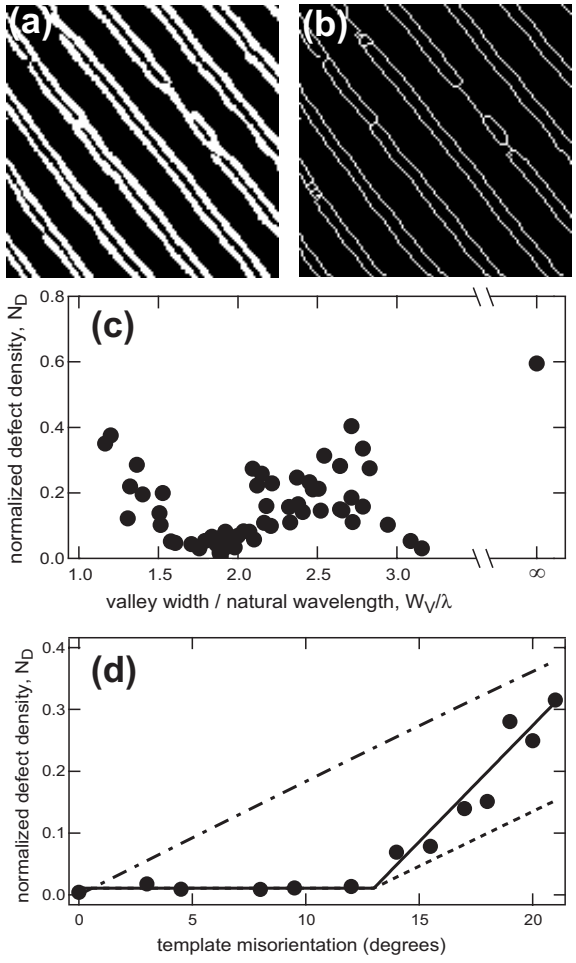

Figure 2. Measurement of the defect density. a) 4 μm × 4 μm (128 pixels × 128 pixels) images following thresholding, and b) thinning of bottom-left quadrant of templated sample appearing in Figure 1d. c) Normalized defect density versus normalized valley width for lithographically templated samples. Vertical error bars are 10% of the base values. d) Normalized defect density versus template boundary misorientation with respect to the direction of the projected ion beam. Valley width 280 ± 24 nm, one ripple per valley. Lines are geometrical models discussed in the text.

than two white neighbors and subtracting the number of ripple ends at the edges of a hypothetically perfect image of the same natural wavelength and scan area. To permit comparison of images with different wavelengths and scan areas, the raw number of defects was multiplied by λ^2 and divided by the area occupied by the ripples excluding the area occupied by the template boundaries. This procedure yielded a dimensionless order parameter that corresponded most closely to our qualitative visual ranking of a wide variety of sputter-rippled samples: those possessing smaller N_D values appear more ordered to the eye and are observed to have fewer dislocation defects in the few cases where we counted them manually.

The reduction in defect density due to templating is illustrated in Figure 2c, in which the normalized defect density is plotted versus the valley width,[24] W_V, divided by natural wavelength. From this figure we make two major observations. First, we observe oscillatory behavior—the defect density is reduced when W_V is near an integer multiple of λ. However, as seen in Figure 1a, when the valley width is about 2λ, only one ripple crest appears, and in Figure 1d, when the valley width is about 3λ, only two ripple crests appear. It appears that the width from which ripples are excluded is greater than the mesa width by about λ in all images.

Second, we observe that for all valley widths studied, including half-integer values, the ripples are less defective than at infinite-valley width. From the data presently available we cannot determine how far apart the templates can be and still significantly decrease the defect density. Figure 1f indicates that templating can still be effective for valley widths of up to 5λ; however, this sample was fabricated differently from the lithographically fabricated samples and therefore cannot be compared directly with them.

The orientation of template boundaries with respect to the direction of the projected ion beam also plays an important role in determining the organization of the ripples. The ripples follow the boundary orientation up to a critical angle of $\phi^* = 13°$ of misorientation without a significant increase in defect density, as shown in Figure 2d. As the misorientation increases further, defects are introduced in proportion to the incremental misorientation. The solid line fitted to the data above ϕ^* has a slope of about 0.038. From a purely geometrical model in which ripples remain parallel to the direction of the projected ion beam and terminate in "defects" where they reach the borders of the valley, one would expect a slope of 0.018 and an intercept of zero, as shown by the dot–dashed curve. From an alternative geometrical model in which ripples rotate up to ϕ^* and remain at ϕ^* misorientation from the ion beam upon further template boundary misorientation, one would expect the response described by the dashed curve. From visual inspection of the defect images, it appears that increasing misorientation beyond ϕ^* results in an increasing break-up of the rotated ripple structure in a patchwise manner, with the patches reverting to the orientation of the ion beam.[25] We expect variations in sputter conditions to lead to variations in ϕ^*, larger values of which provide, in principle, a greater flexibility to control the pattern appearing within an area by controlling only its perimeter. We anticipate no orientation limit for 2D dot patterns that result from normal-ion incidence.[3,26]

Guided self-organization of these lithographically templated samples occurs on the valleys of the templated structure and not on the mesas. This may occur because the mesa width is not much greater than λ: there is no clear-cut way to distinguish a

ADVANCED MATERIALS

ripple-free mesa from a mesa with exactly one ripple ridge and no ripple troughs. For the FIB-templated samples we observe ripples on the mesas that are significantly wider than any of the lithographically fabricated mesas. Ripples are likely to form on sufficiently wide lithographically templated mesas as well.

Two theoretical approaches may potentially lead to an understanding of the templating effect of the boundaries. A nonlinear sputter morphology evolution theory for morphologies with tall, steep walls might be applied to the entire morphology. Currently none is available, as all useable models expand the morphology in powers of the surface slope, which is treated as a small parameter. Alternatively, the walls might be treated as a boundary condition on the evolution of initially flat valleys. In this case, the initial evolution might be accurately modelled as linear, and nonlinear behavior may or may not be important in determining the topographies observed.

A linear perturbation theory[27] correctly predicts many aspects[16] of the formation of ripples but does not explain others,[3,17,28] such as the amplitude saturation at long times. Based on previous work,[17] we know that for the present conditions the amplitude of the ripples is approaching saturation, indicating that their behavior may be beyond that describable by the linear theory. The addition of nonlinear sputter effects[29] may account for this behavior; however, in the absence of theoretical predictions of an experimentally detectable signature that uniquely distinguishes them, nonlinear effects are not understood in any systematic manner. The consequences of nonlinear behavior for lateral templating constitute an important area for further study. In particular, we expect nonlinear behavior to be the key to two important aspects of this phenomenon: the maximum range of the lateral-templating effect and the extent to which one can control the morphology of such a self-organization process by controlling only the boundaries of the area in which the process develops.

In conclusion, we have shown that self-organized sputter patterns can be effectively guided by lateral templating. The degree of organization can be controlled by changing the spacing and orientation of pre-patterned boundaries made on the substrate. This effect contributes to a developing paradigm for hierarchical mass production of nanoscale 2D and 3D architectures. The measurements may also provide an excellent basis for testing and further development of nonlinear models of morphological evolution under ion sputtering in particular, and of driven systems in general.

Experimental

Pre-patterned Si(001) substrates were produced by electron-beam lithography followed by reactive-ion etching or by drilling trenches with a FIB. Lithographically fabricated patterns consisted of arrays of parallel mesas and valleys of varying spacing. The mesa height of 110 nm was obtained by reactive-ion etching for 3.5 min under CF_4 gas. The periodicity varied from 400 to 800 nm. The valley width varied from 160 to 450 nm. For FIB patterning, ~500 nm deep trenches with 1 μm periodicity were drilled with a 30 keV Ga^+ FIB with beam current of 1 pA and a nominal beam diameter of 6 nm. The patterned substrate was then introduced into a ultrahigh vacuum (UHV) sputter patterning chamber, working at a base pressure of 2×10^{-10} torr (1 torr = 133.32 Pa). The pre-existing pattern was aligned with the direction of the projected ion beam using optical diffraction. The surface was bombarded with 1 keV Ar^+ from a collimated 3 cm Kaufman ion gun differentially pumped and working at 10^{-4} torr. The sample was heated at 540 °C and the angle between the beam and the sample normal was 45°. The typical ion flux was 0.4 mA cm^{-2}. The sputtering time was 45 min unless indicated otherwise. Post-irradiated surfaces were observed in air using AFM in intermittent contact mode. Because only a fraction of the area under the uniform central portion of the ion beam was patterned, a comparison could be made between sputter ripple morphologies inside and outside the pre-patterned region under otherwise identical conditions in the same run.

Received: April 7, 2005
Final version: June 30, 2005
Published online: October 5, 2005

[1] C. Teichert, M. G. Lagally, L. J. Peticolas, J. C. Bean, J. Tersoff, *Phys. Rev. B* **1996**, *53*, 16 334.
[2] M. Park, C. Harrison, P. M. Chaikin, R. A. Register, D. H. Adamson, *Science* **1997**, *276*, 1401.
[3] S. Facsko, T. Dekorsy, C. Koerdt, C. Trappe, H. Kurz, A. Vogt, H. L. Hartnagel, *Science* **1999**, *285*, 1551.
[4] R. D. Twesten, D. M. Follstaedt, S. R. Lee, E. D. Jones, J. L. Reno, J. M. Millunchick, A. G. Norman, S. P. Ahrenkiel, A. Mascarenhas, *Phys. Rev. B* **1999**, *60*, 13 619.
[5] a) V. A. Shchukin, D. Bimberg, *Rev. Mod. Phys.* **1999**, *71*, 1125. b) T. Thurn-Albrecht, J. Schotter, C. A. Kastle, N. Emley, T. Shibauchi, L. Krusin-Elbaum, K. Guarini, C. T. Black, M. T. Tuominen, T. P. Russell, *Science* **2000**, *290*, 2126.
[6] a) R. D. Peters, X. M. Yang, Q. Wang, J. J. de Pablo, P. F. Nealey, *J. Vac. Sci. Technol., B* **2000**, *18*, 3530. b) L. Rockford, S. G. J. Mochrie, T. P. Russell, *Macromolecules* **2001**, *34*, 1487. c) R. A. Segalman, H. Yokoyama, E. J. Kramer, *Adv. Mater.* **2001**, *13*, 1152. d) O. G. Schmidt, S. Kiravittaya, Y. Nakamura, H. Heidemeyer, R. Songmuang, C. Muller, N. Y. Jin-Phillipp, K. Eberl, H. Wawra, S. Christiansen, H. Grabeldinger, H. Schweizer, *Surf. Sci.* **2002**, *514*, 10. e) S. O. Kim, H. H. Solak, M. P. Stoykovich, N. J. Ferrier, J. J. de Pablo, P. F. Nealey, *Nature* **2003**, *424*, 411. f) J. Y. Cheng, A. M. Mayes, C. A. Ross, *Nat. Mater.* **2004**, *3*, 823.
[7] A. Karmous, A. Cuenat, A. Ronda, I. Berbezier, S. Atha, R. Hull, *Appl. Phys. Lett.* **2004**, *85*, 6401.
[8] B. Yang, F. Liu, M. G. Lagally, *Phys. Rev. Lett.* **2004**, *92*, 025 502.
[9] J. Aizenberg, A. J. Black, G. M. Whitesides, *Nature* **1998**, *394*, 868.
[10] a) D. K. Yi, E. M. Seo, D. Y. Kim, *Appl. Phys. Lett.* **2002**, *80*, 225. b) J. P. Hoogenboom, C. Retif, E. de Bres, M. V. de Boer, A. K. van Langen-Suurling, J. Romijn, A. van Blaaderen, *Nano Lett.* **2004**, *4*, 205.
[11] P. Sutter, E. Sutter, P. Rugheimer, M. G. Lagally, *Surf. Sci.* **2003**, *532*, 789.
[12] P. Sutter, E. Mateeva, M. G. Lagally, *J. Vac. Sci. Technol., B* **1998**, *16*, 1560.
[13] J. L. Gray, S. Atha, R. Hull, J. A. Floro, *Nano Lett.* **2004**, *4*, 2447.
[14] M. Navez, D. Chaperot, C. Sella, *C. R. Hebd. Seances Acad. Sci.* **1962**, *254*, 240.
[15] a) G. Carter, V. Vishnyakov, M. J. Nobes, *Nucl. Instrum. Methods Phys. Res., Sect. B* **1996**, *115*, 440. b) F. Frost, A. Schindler, F. Bigl, *Phys. Rev. Lett.* **2000**, *85*, 4116.
[16] J. Erlebacher, M. Aziz, E. Chason, M. Sinclair, J. Floro, *Phys. Rev. Lett.* **1999**, *82*, 2330.
[17] J. Erlebacher, M. J. Aziz, E. Chason, M. B. Sinclair, J. A. Floro, *J. Vac. Sci. Technol., A* **2000**, *18*, 115.
[18] S. Rusponi, C. Boragno, U. Valbusa, *Phys. Rev. Lett.* **1997**, *78*, 2795.
[19] a) T. M. Mayer, E. Chason, A. J. Howard, *J. Appl. Phys.* **1994**, *76*, 1633. b) C. C. Umbach, R. L. Headrick, K. C. Chang, *Phys. Rev. Lett.* **2001**, *87*, 246 104.

[20] a) M. C. Cross, P. C. Hohenberg, *Rev. Mod. Phys.* **1993**, *65*, 851. b) P. Bellon, R. S. Averback, *Scr. Mater.* **2003**, *49*, 921.
[21] WSxM free software downloadable at http://www.nanotec.es
[22] http://rsb.info.nih.gov/ij/download.html
[23] N. Otsu, *IEEE Trans. Syst. Man. Cybern.* **1979**, *9*, 62.
[24] W_V was determined as follows. From a histogram of the heights of surface features on a templated sample, we identified a threshold to create binary images of template ridge tops and valleys. The resulting images, made up of alternating black and white stripes, were Fourier transformed—the templating period was determined from the reciprocal of the distance between any two spots. The "boundary width", W_B, of the white (ridge top) stripes was obtained by fitting a sine cardinal (sinc) function to the envelope of intensities at the diffraction spots corresponding to the template periodicity. The valley width, W_V, was evaluated as the difference between the template period and W_B.
[25] We have verified that when the boundary disorientation is much greater than ϕ^* (e.g., 60°), the pattern has reverted to an ordered array of topological defects with ND falling near the dot–dashed line, as expected from non-rotating ripples.
[26] R. Gago, L. Vazquez, R. Cuerno, M. Varela, C. Ballesteros, J. M. Albella, *Appl. Phys. Lett.* **2001**, *78*, 3316.
[27] a) R. M. Bradley, J. M. Harper, *J. Vac. Sci. Technol., A* **1988**, *6*, 2390. b) P. Sigmund, *Phys. Rev.* **1969**, *184*, 383.
[28] S. Habenicht, W. Bolse, K. P. Lieb, K. Reimann, U. Geyer, *Phys. Rev. B* **1999**, *60*, R2200.
[29] a) R. Cuerno, H. A. Makse, S. Tomassone, S. T. Harrington, H. E. Stanley, *Phys. Rev. Lett.* **1995**, *75*, 4464. b) S. Park, B. Kahng, H. Jeong, A.-L. Barabasi, *Phys. Rev. Lett.* **1999**, *83*, 3486. c) M. A. Makeev, R. Cuerno, A.-L. Barabasi, *Nucl. Instrum. Methods Phys. Res., Sect. B* **2002**, *197*, 185.

Incorporation of Point Defects into Self-Assembled Three-Dimensional Colloidal Crystals**

By *Qingfeng Yan*, *Ao Chen*, *Soo Jin Chua*, and *Xiu Song Zhao**

Photonic crystals (PCs) or photonic bandgap (PBG) materials offer a promising platform for future photonic integrated circuits (PICs) and optoelectronic integrated circuits (OEICs).[1–3] Three-dimensional (3D) PCs with a full PBG allow one to control the flow of light omnidirectionally. Currently, there are mainly two methods for fabricating 3D PCs, i.e., "top–down" lithography and "bottom–up" self assembly. The former utilizes conventional semiconductor micromachining techniques, such as electron-beam lithography (EBL) and inductively coupled plasma (ICP) etching, to fabricate 3D periodical structures in a layer-by-layer manner. Many photonic applications, such as optical microcavities and waveguides, require an exact placement of well-defined artificial defects (e.g., planar, line, and point defects) within 3D PCs.[4–7] Although the "top–down" method has been demonstrated to work for the insertion of artificial defects into 3D PCs, it is relatively expensive, tedious, and time-consuming, with a low throughput, and is applicable only to limited structures.[8–10] On the other hand, the "bottom–up" method, which is based on the self-assembly of colloidal microspheres, provides a simple and inexpensive approach to the fabrication of 3D PCs.[11] Unfortunately, the introduction of artificial defects using the "bottom–up" method is not as straightforward as it is in the case of using the "top–down" method. Defect engineering in self-assembled 3D PCs thus has been a great challenge.

A layer-by-layer deposition strategy for the insertion of planar defects in self-assembled 3D PCs has been described.[12] The chemical vapor deposition (CVD) technique has also been demonstrated to place dielectric planar defects in 3D PCs.[13,14] Multiphoton photopolymerization[15] and a direct electron-beam writing technique[16] have been employed to construct deterministic defects in self-assembled 3D PCs. Ozin and co-workers[17] have described the fabrication of a micrometer-scale line defect on the surface of an inverse silicon PC by modification of the local refractive index using laser direct writing and microannealing techniques. Very recently, the same group[18] and our group[19] have demonstrated a straightforward method to embed micrometer-scale line defects within the interior of a self-assembled 3D PC by using conventional optical photolithography and self-assembly techniques.

Many photonic applications, such as microcavities of a high quality factor (Q) in low-threshold lasers and light-emitting diodes, require the presence of point defects in a PC.[6–8,10] Introducing point defects into 3D PCs has proven quite difficult, with only a few examples reported.[8–10,20–25] By using a layer-by-layer lithographic method, 3D silicon[8] and GaAs PCs[10] with designed point defects have recently been fabricated. Matthias et al.[9] have demonstrated the possibility of introducing point defects into a 3D silicon PC by using modified electrochemical etching and lithographic methods. Direct laser writing has been described to produce point defects within polymer 3D PCs fabricated by using holographic lithography.[20] For self-assembled 3D PCs, the introduction of point defects has been reported by doping a system with impure colloidal spheres, of different sizes or dielectric strengths, during the self-assembling process.[21–24] However, such point defects are randomly distributed throughout the structure. For practical device applications, the position of the point defects should be controllable. For self-assembled polymer colloidal crystals (opals) from poly(methyl methacrylate)

[*] Prof. X. S. Zhao, Dr. Q. Yan
Department of Chemical and Biomolecular Engineering
National University of Singapore
10 Kent Ridge Crescent, 119260 (Singapore)
E-mail: chezxs@nus.edu.sg
A. Chen, Prof. S. J. Chua
Department of Electrical and Computer Engineering
National University of Singapore
10 Kent Ridge Crescent, 119260 (Singapore)

[**] This work was supported by the Agency for Science, Technology and Research (A STAR) of Singapore under grant number 0221090060 and the Nippon Sheet Glass Foundation.

 DOI: 10.1002/adma.200501065